European Journal of Pharmaceutics and Biopharmaceutics 79 (2011) 612–620

Contents lists available at ScienceDirect

European Journal of Pharmaceutics and Biopharmaceutics

journal homepage: www.elsevier.com/locate/ejpb

Research paper

Interaction of an amphiphilic squalenoyl prodrug of gemcitabine with cellular membranes

L. Bildstein [a,b,*,1], B. Pili [a,b,1], V. Marsaud [a,b], S. Wack [a,b], F. Meneau [c], S. Lepêtre-Mouelhi [d,b], D. Desmaële [d,b], C. Bourgaux [a,b], P. Couvreur [a,b], C. Dubernet [a,b]

[a] Univ. Paris-Sud, UMR CNRS 8612, Faculté de Pharmacie, Châtenay-Malabry, France
[b] CNRS, Châtenay-Malabry, France
[c] Synchrotron SOLEIL, L'Orme des Merisiers, Gif-sur-Yvette, France
[d] Univ. Paris-Sud, UMR CNRS 8076 BIOCIS, Faculté de Pharmacie, Châtenay-Malabry, France

ARTICLE INFO

Article history:
Received 8 November 2010
Accepted in revised form 8 July 2011
Available online 19 July 2011

Keywords:
Gemcitabine
Squalene
Prodrug
Membrane permeabilization
Hemolysis
Nonlamellar phases

ABSTRACT

We have designed an amphiphilic prodrug of the anticancer agent gemcitabine (dFdC), by covalent coupling to squalene. This bioconjugate, which self-assembled into nanoparticles (NPs) in water, was previously found to display an impressive anticancer activity both *in vitro* and *in vivo*. The present study aims to investigate the impact of SQdFdC nanoparticles on cellular membranes. MTT assays showed that, in the nanomolar range, squalenoyl gemcitabine (SQdFdC) was slightly less active than dFdC on a panel of human cancer cell lines, *in vitro*. However, above 10 μmol L^{-1} SQdFdC was considerably more cytotoxic than dFdC. Contrarily to its parent drug, SQdFdC also induced cell lysis in a few hours, as evidenced by LDH release assays. Erythrocytes were used as an experimental model insensitive to the antimetabolic activity of dFdC to further investigate the putative membrane-related cytotoxic activity of SQdFdC. The bioconjugate also induced hemolysis in a time- and dose-dependent fashion, unlike squalene or dFdC, which clearly proved that SQdFdC could permeabilize cellular membranes. Structural X-ray diffraction and calorimetry studies were conducted in order to elucidate the mechanism accounting for these observations. They confirmed that SQdFdC could be transferred from NPs to phospholipid bilayers and that the insertion of the prodrug within model membranes resulted in the formation of nonlamellar structures, which are known to promote membrane leakage. As a whole, our results suggested that due to its amphiphilic nature, the cell uptake of SQdFdC resulted in its insertion into cellular membranes, which could lead to the formation of nonlamellar structures and to membrane permeation. Whether this mechanism could be the source of toxicity *in vivo*, however, remains to be established, since preclinical studies have clearly proven that squalenoyl gemcitabine displayed a good toxicity profile.

1. Introduction

Gemcitabine (2′,2′-difluorodeoxycytidine, dFdC) is a cytidine analog currently used in clinic against a number of solid tumors. Over the past 15 years, it has been approved for the treatment of locally advanced or metastatic non-small-cell lung cancer gemcitabine plus cisplatin versus cisplatin alone in patients [1] and pancreatic cancer [2], invasive bladder cancer [3] and in second-line against metastatic breast cancer [4]. Phase II clinical trials of this anticancer agent have also been undertaken against cervix [5,6] and colorectal malignancies [7]. The drug exerts its cytostatic and cytotoxic activities mainly through the incorporation of its triphosphate metabolite into elongating DNA, which leads to chain termination, cell cycle blockage and eventually apoptosis [8]. The uptake of dFdC via membrane transporters [9] and its phosphorylation by cytoplasmic kinases are critical prerequisites of this process, and their impairment may lead to the induction of resistance to the chemotherapy [10]. dFdC also undergoes a rapid deamination into its inactive uracil derivative in the bloodstream, which severely limits its bioavailability [11].

We have introduced the concept of "squalenoylation" to improve the efficacy of gemcitabine and to circumvent some of its above-mentioned shortcomings. Squalene (SQ), a natural lipidic precursor of the biosynthesis of cholesterol, was coupled to the amino group of the cytosine nucleus of dFdC. When introduced in water, the resulting bioconjugate spontaneously self-assembled

Abbreviations: dFdC, gemcitabine; DPPC, dipalmitoylphosphatidylcholine; DSC, differential scanning calorimetry; LDH, lactate dehydrogenase; LISB, low ionic strength buffer; MLV, multilamellar vesicles; NP, nanoparticle; SAXS/WAXS, small/wide angle X-ray scattering; SQ, squalene; SQdFdC, squalenoyl gemcitabine.

* Corresponding author. Univ. Paris-Sud, UMR CNRS 8612, IFR 141-ITFM, Faculté de Pharmacie, Châtenay-Malabry F-92296, France. Tel.: +33 146835573.
E-mail address: lucien.bildstein@gmail.com (L. Bildstein).

[1] These authors have equally participated to this work.

0939-6411/$ - see front matter © 2011 Elsevier B.V. All rights reserved.
doi:10.1016/j.ejpb.2011.07.003

into nanoparticles (NPs) [12], which were found dramatically more active than dFdC against murine leukemia models, *in vivo* [13]. Mechanistic studies have proven that squalenoyl gemcitabine (SQdFdC) was not a substrate of the membrane transporters of dFdC [14] but that it rather entered cells by an albumin-enhanced passive diffusion [15]. Structural studies have underlined that the amphiphilic SQdFdC molecules strongly interacted with phospholipids [16], and we have recently reported that cellular membranes constituted the main intracellular reservoir of the prodrug [17].

Numerous authors have indicated that other amphiphilic drugs could interact with cellular membranes [18], which could lead to toxic side effects [19–21]. We, therefore, investigated whether the interaction of squalenoyl gemcitabine with cellular membranes could result in cytotoxic effects caused by their disruption. The cytostatic and cytotoxic activities of SQ, dFdC, and SQdFdC were compared on a panel of human cancer cell lines, *in vitro*. The cytolytic effects of SQdFdC were clearly evidenced, and their dependency with time and drug concentration was assessed on both cancer cell lines and erythrocytes. In addition, differential scanning calorimetry was performed and X-ray diffraction measurements were taken, demonstrating the ability of SQdFdC to be transferred from NPs to DPPC model membranes, which leads to the formation of nonlamellar structures responsible for the enhanced membrane permeability and cell lysis.

2. Materials and methods

2.1. Chemicals and drugs

Ethanol was purchased from Carlo Erba (Italy), all cell culture media from Lonza (France), and other chemicals, including Squalene, from Sigma–Aldrich (France). Ultrapure MilliQ® water was used (Millipore, France). Gemcitabine hydrochloride (dFdC) was obtained from Sequoia Research Products Ltd. (UK). SQdFdC was synthesized, purified, and characterized as previously reported [12]. 1,2-Dipalmitoyl-sn-3-phosphatidylcholine (DPPC) (molecular weight of 733.56, purity 99%) was purchased from Avanti Polar Lipids (Alabaster, Alabama, USA) and used without further purification.

2.2. Preparation of SQdFdC NPs and control SQ dispersions

Two milligrams of SQdFdC was dissolved in 1 mL ethanol and added dropwise under vigorous magnetic stirring to 2 mL of MilliQ® water to generate nanoparticles (NPs). Two milligrams of SQ was dispersed similarly, in the presence of 1% (w/v) Pluronic F68, to stabilize the SQ emulsion. Ethanol was evaporated on a Rotavapor® (Büchi) to reach a final volume of 2 mL. The resulting nano-objects were characterized by quasi-elastic light scattering on a Zetasizer Nano ZS (Malvern) in terms of average diameter (Z-avg) and polydispersity index (Pdi). Typical characteristics of the objects were the following: SQdFdC NPs, Z-avg = 104 ± 1 nm; Pdi = 0.084 ± 0.012 and SQ dispersion, Z-avg = 304 ± 2 nm; Pdi = 0261 ± 0.001. The dispersions were diluted in culture media and added onto cells within 1 h after their preparation.

2.3. Cell lines and culture conditions

The human cell lines MCF-7 and MDA-MB-231 (breast adenocarcinoma), HT-29 (colorectal adenocarcinoma), and KB-3-1 (cervix carcinoma) were grown in Dulbecco's Modified Eagle Medium (DMEM) Hi-Glucose GlutaMAX, in the presence of fetal calf serum (FCS, 10% (v/v)). The human leukemia cell line CCRF CEM was cultured in RPMI 1640/GlutaMAX with 10% (v/v) FCS. Cell culture media were supplemented with penicillin (50 U mL^{-1}) and streptomycin (50 μg mL^{-1}). Cells were grown in a 5% CO_2 humidified atmosphere at 37 °C.

2.4. MTT assay

Cytostatic and cytotoxic effects were monitored thanks to the 3-[4,5-dimethylthiazol-2-yl]-3,5-diphenyl tetrazolium bromide (MTT) test. Cells were seeded in 96-wells plates, and drug-containing media were added to the exponentially growing cells the day after. After a 48 h exposure to the drugs, each well received MTT (final concentration 0.5 mg mL^{-1}). Two hours later, the plates were centrifuged and the supernatants replaced by DMSO to dissolve the formazan crystals. Absorbance at 570 nm, which is proportional to the number of living cells, was measured on a Metertech Σ 960 microplate reader (Fisher Bioblock). Viability data normalized to exponentially growing untreated control cells were fit either to a Hill function with an additive constant (dFdC) or to a sum of two Hill functions (SQdFdC), by nonlinear least squares on Excel® software (Microsoft) thanks to its built-in "Solver" algorithm.

2.5. LDH release assay

The membrane disruption of human cancer cells was investigated using the lactate dehydrogenase (LDH, a stable cytoplasmic enzyme) release assay thanks to a commercial colorimetric kit (Cytotox 96 nonradioactive assay, Promega, France), according to manufacturer's instructions. Briefly, the supernatant of cells seeded in 96-well plates was replaced by fresh media containing 200 μmol L^{-1} of either dFdC or SQdFdC NPs. After various incubation times at 37 °C, the supernatants were homogenized, plates were centrifuged, and samples were taken for LDH measurement. The cell lysis was calculated relatively to untreated control cells and to cells entirely lysed by 1% (v/v) Triton X100.

2.6. Hemolysis experiments

These experiments were carried out in a cell-compatible low ionic strength buffer (LISB) in order to maintain the colloidal stability of the NPs in a protein-free environment [15]. Control dynamic light scattering measurements carried out either in MilliQ® water, LISB- or FCS-containing culture medium have shown that the colloidal stability of the NPs was similar in all cases. LISB composition was as follows: 250 mmol L^{-1} saccharose, 10 mmol L^{-1} glucose, 15 mmol L^{-1} HEPES buffer, 90 μmol L^{-1} Ca^{2+} and 50 μmol L^{-1} Mg^{2+}, pH set to 7.4. Healthy adult female CD2F1/NCrl mice were anaesthetized by intraperitoneal injection of a ketamine/xylazine solution (resp. 33 mg kg^{-1} and 7 mg kg^{-1}), and their blood was sampled by cardiac puncture, in compliance with the European Community guiding principles in the care and use of animals (86/609/CEE, CE Off J No. L358, 18 December 1986). The erythrocytes were separated from serum by centrifugation, washed twice in 10 volumes of LISB, and dispersed in drug-containing LISB according to an hematocrite (erythrocyte volume fraction) of 0.1%, 0.2% or 0.28%. Cell suspensions were incubated at 37 °C and harvested each hour for up to 6 h. The optical density of the media was then assessed at a wavelength of 450 nm on a microplate reader, after removing the cellular bodies by centrifugation. Hemolysis percentage was calculated relatively to the absorbance obtained for erythrocytes in the presence of 1% (v/v) Triton X100 (100% lysis). The order of magnitude of the amount of lipids contained in the hemolysis setup was estimated on the basis of published data [22–26], for comparison to the SQdFdC/DPPC ratio used in DSC-SAXS/WAXS studies.

2.7. Preparation of the SQ/DPPC mixture

A dry film from a mixture of DPPC and squalene was hydrated to evaluate whether SQ interacted with DPPC multilamellar vesicles (MLVs). Briefly, chloroform stock solutions of DPPC and SQ were mixed to obtain the chosen molar fractions r = [SQ]/[DPPC] between 0.05 and 2. Samples were dried under nitrogen stream and then submitted to low-vacuum freeze drying. The dry films were hydrated in excess (80%, w/w) with ultrapure Millipore water. The suspensions were heated at 50 °C, above the chain melting transition temperature of DPPC, and vortexed in order to obtain homogenous suspensions.

An aliquot of the samples (about 10 mg) was loaded either into DSC hermetically sealed aluminum pans (50 μL, Perkin-Elmer, Waltham, Massachusetts, USA) or in quartz capillaries (external diameter 1.4 ± 0.1 mm, wall thickness 0.01 mm) (Glas, Müller, Berlin, Germany).

2.8. Dispersions containing SQdFdC nanoparticles and DPPC liposomes

We generated a dispersion containing SQdFdC NPs and DPPC MLVs at the same time, in order to investigate the transfer of SQdFdC molecules from the NPs to the MLVs. To achieve this, the dry DPPC powder (about 20 mg of anhydrous lipid) was dissolved in chloroform. The solvent was evaporated under a nitrogen stream, followed by low-vacuum freeze drying. The dry film was hydrated in excess (>80%, w/w) with an aliquot of a concentrated SQdFdC NPs suspension (5 mg mL^{-1}), prepared by nanoprecipitation as described above, to obtain a final molar ratio r = [SQdFdC]/[DPPC] = 0.09. The suspension was vortexed to achieve mixing of MLVs and NPs. Aliquots of the samples were loaded into DSC aluminum pans or in quartz capillaries as described above.

2.9. Differential scanning calorimetry

The thermal analysis has been carried out using a DSC 7 (Perkin-Elmer, Inc.) equipped with a cooling device (Intracooler II) in dry air atmosphere. The instrument was standardized using the enthalpy and melting point of lauric acid (99.5% purity, T_m = 43.7 °C; ΔH_m = 35.713 kJ mol^{-1}) [27]. Data analysis has been performed using TA Universal Analysis program (New Castle, Delaware, USA). The transition temperatures were taken at the onset of the transitions (T_{onset}), i.e., the intersection of the tangent to the left side of the endothermic peak with the baseline. The enthalpy (ΔH) of the transitions was obtained from the area under the peaks.

2.10. X-ray diffraction

X-ray scattering experiments were performed on the Austrian synchrotron beamline at ELETTRA and on the SWING synchrotron beamline at SOLEIL. The experiments were carried out either at 20 °C or at 50 °C, respectively, below or above the main transition temperature of DPPC. The scattered intensity was reported as a function of the scattering vector $q = 4\pi\sin\theta/\lambda$, where 2θ is the scattering angle and λ the wavelength of the incident beam. For both instruments, the calibration of the q-range was carried out with pure tristearine ($2L\beta$ form) and silver behenate. Samples, loaded in quartz capillaries, were thermostated in a homemade microcalorimeter, Microcalix, designed to allow simultaneous DSC and X-ray diffraction measurements.

3. Results

3.1. Cytostatic and cytotoxic activities of dFdC and SQdFdC

The effect of a 48-h long, continuous exposure to dFdC or SQdFdC, was assessed on the human cancer cell lines MCF-7, MDA-MB-231 (breast), HT-29 (colorectal), and KB-3-1 (cervix) by means of the MTT test. Below 10,000 nmol L^{-1}, dFdC and SQdFdC induced cytostasis on all cell lines (see Fig. 1A for KB-3-1 and Fig. 1B for MDA-MB-231), as shown by the decrease in viability followed by a plateau observed around 50% cell viability (Fig. 1A) or 70–75% cell viability (Fig. 1B). Depending on the cell line, the onset of this cytostatic effect occurred between 5 and 50 nmol L^{-1} in the case of dFdC and between 50 and 200 nmol L^{-1} for SQdFdC. Noteworthy, above 10,000 nmol L^{-1} of SQdFdC, a strong cytotoxic effect was observed in both cell lines.

Additional MTT assays were performed on the MCF-7 and HT-29 cell lines to investigate whether the cytotoxicity of SQdFdC observed above 10 μmol L^{-1} could be attributed to squalene (SQ) or not. In this view, a physical mixture of dFdC to a SQ dispersion at an equivalent concentration was also investigated. SQ slightly reduced the viability of MCF-7 cells, in an erratic manner (Fig. 2), but control experiments showed that the effect could rather be attributed to the pluronic F68 added to the SQ to ensure its dispersion in aqueous media than to SQ itself (data not shown). The physical mixture of SQ and dFdC had the same impact on cellular viability than dFdC alone. Similar results were obtained on the HT-29 cell line (data not shown).

3.2. Cell lysis induced by dFdC and SQdFdC

The short-term lytic properties of SQdFdC and dFdC at high concentrations were investigated by monitoring the release of a cytoplasmic marker (lactate dehydrogenase, LDH). These experiments were carried out on cell lines that exhibited either a cytostatic or a cytotoxic response to dFdC in our experimental conditions (resp. the MCF-7 cell line and the CCRF CEM human leukemia cell line). While 200 μmol L^{-1} of dFdC induced no observable cell lysis over a 6-h-long incubation on both cell lines, the same concentration of SQdFdC NPs permeabilized the membranes of CCRF CEM cells (Fig. 3), in a very significant manner ($P < 0.05$ by two-tailed heteroscedastic t-tests). MCF-7 cells were also lysed by SQdFdC, although the onset of the lysis was delayed by several hours.

3.3. Drug-induced hemolysis

Erythrocytes collected on healthy mice were used as a cellular model to specifically investigate the membrane disruption induced by SQdFdC, dFdC, and SQ. Hemolysis experiments were performed in the absence of proteins, in a NP-compatible isotonic buffer. Fig. 4 reports typical hemolysis kinetics obtained in the presence of SQ, dFdC, and SQdFdC. No hemolysis was observed in the presence of pure SQ at 20 μmol L^{-1}. dFdC alone induced a slight hemolysis, which was not concentration-dependent (5, 20 or 100 μmol L^{-1} of dFdC, data not shown). On the contrary, SQdFdC induced a considerable hemolysis (from 3 h onwards, significant differences were found between control and SQdFdC-treated erythrocytes, $P < 0.05$ by two-tailed heteroscedastic t-tests), in a dose- and time-dependent fashion (Fig. 4).

The SQdFdC concentration leading to 50% hemolysis in the presence of various erythrocyte volume fractions (Hematocrite, Ht) was also investigated. The results presented in Table 1 indicated that increasing the cell density decreased the lysis percentage. Indeed, the amount of SQdFdC required to achieve median hemolysis was linearly correlated with the hematocrite.

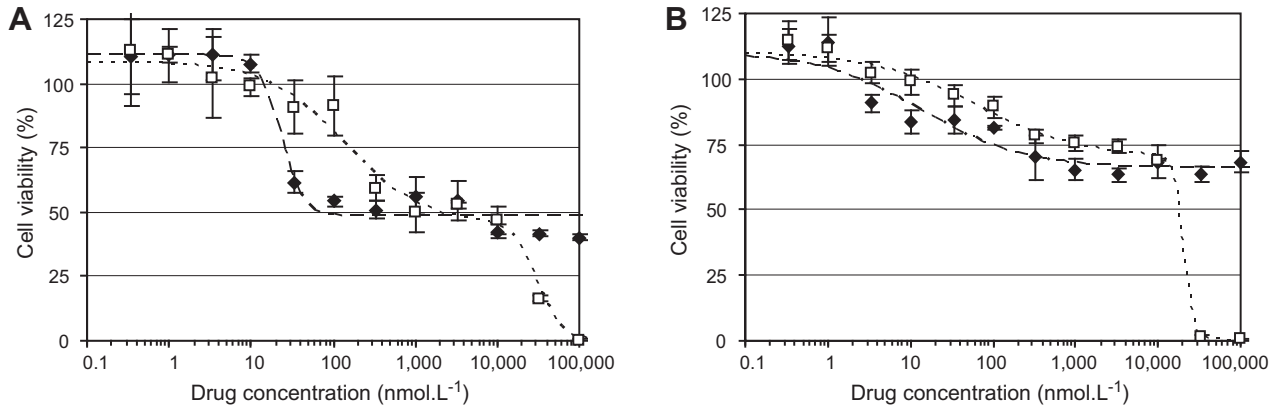

Fig. 1. Cytostatic and cytotoxic effects of a 48-h exposure to dFdC (♦) or SQdFdC (□) of (A) KB-3-1 and (B) MDA-MB-231 cell lines, measured by MTT assay. The results are reported as mean ± SD over triplicate measurements and are representative of at least two independent experiments. The lines are the graphical representation of Hill-based functions fit to each experimental data set.

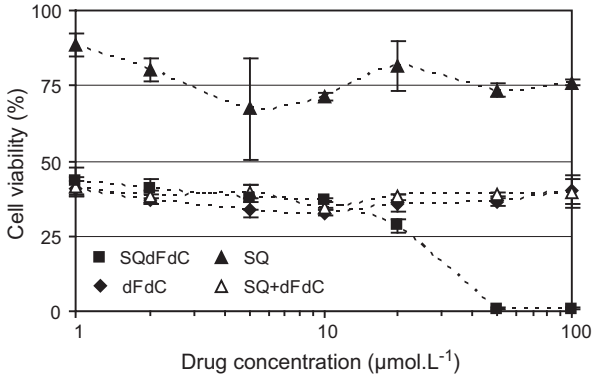

Fig. 2. Cytostatic and cytotoxic effects of SQdFdC and dFdC on MCF-7 measured by MTT assay and compared with those of SQ and the physical mixture of SQ + dFdC. The results are reported as mean ± SD over triplicate measurements and are representative of two independent experiments.

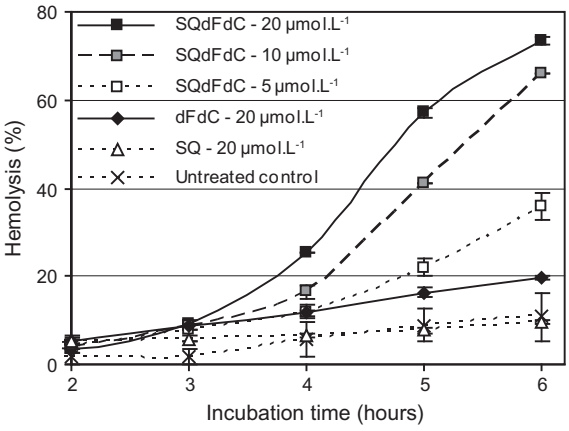

Fig. 4. Hemolytic activity of dFdC (diamonds), SQ (triangles), and SQdFdC (squares, various concentrations), comparatively to untreated erythrocytes (crosses), at a 0.2% hematocrite. The results are reported as mean ± SD over triplicate measurements and are representative of two independent experiments.

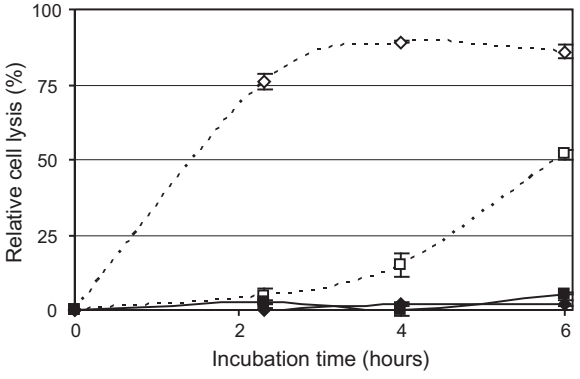

Fig. 3. Lysis of CCRF CEM (♦◇) and MCF-7 (■□) resulting from the exposure to 200 µmol L^{-1} dFdC (full symbols) or SQdFdC (open symbols), measured by LDH release assay. The results are reported as mean ± SD over duplicate measurements and are representative of two independent experiments.

Table 1
SQdFdC concentration resulting in 50% of the maximal hemolysis, after 5 or 6 h of incubation with erythrocyte dispersions at an hematocrite (Ht) of 0.1%, 0.2%, or 0.28%.

Incubation time	[SQdFdC] leading to 50% hemolysis at various hematocrites (µmol L^{-1})		
	Ht = 0.1%	Ht = 0.2%	Ht = 0.28%
5 h	11.7	13.7	15.3
6 h	2.7	6.9	11.2

3.4. Interaction of squalene with model phospholipid bilayers

The effect of squalene and of SQdFdC nanoparticles on DPPC model membranes has been investigated with the aim to better understand the cytotoxic and hemolytic activities of SQdFdC. A previous report had shown that, at physiological pH, the parent drug gemcitabine did not modify the structural and thermal properties of DPPC bilayers [28].

DPPC was chosen as a simple model membrane because phosphatidylcholines are, with sphingomyelins, among the major lipid components of the cellular plasma membranes. Their structure and thermal transitions are well defined, which is an essential prerequisite to investigate a possible membrane perturbation by host molecules. Moreover, DPPC phase transitions occur in a readily accessible temperature range, which enables the study of the influence of the lipid state on interactions.

The highly hydrophobic character of squalene (SQ) suggested that this natural lipid might be incorporated into phospholipid bilayers. Like n-alkanes, SQ could conceivably be inserted either between the chains or in the bilayer center, parallel to the plane

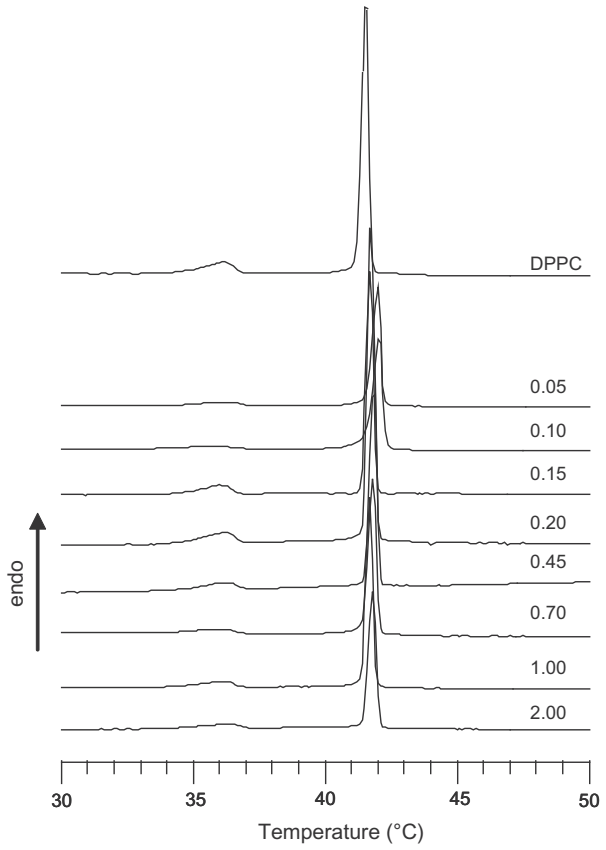

Fig. 5. DSC scans of DPPC and SQ/DPPC mixtures. The molar ratio r = [SQ]/[DPPC] is indicated on the corresponding curve. The thermograms were recorded at 2 °C min^{-1}.

of the membrane. Whether SQ could interact with DPPC model membranes was investigated through DSC and SWAXS measurements. Fig. 5 shows the DSC curves of fully hydrated DPPC and SQ/DPPC mixtures recorded at 2 °C/min. Molar ratios r = [SQ]/[DPPC] in the range 0.05–2 were investigated. All curves were similar. The weak pretransition between the Lβ′ lamellar gel phase and the Pβ′ ripple phase was followed by the Pβ′ to Lα fluid lamellar phase main transition. The onset temperature and the width of the main transition, indicative of the cooperativity of the transition, remained unchanged in the presence of SQ. Only the melting enthalpy decreased slightly with increasing SQ content.

Fig. 6 displays the SAXS patterns of these samples recorded at 20 °C, below the pretransition, and at 50 °C, above the main transition. All X-ray patterns were found identical whatever the amount of SQ and were characteristic, respectively, of the Lβ′ and Lα phases of DPPC. The lamellar spacing, deduced from the position of the SAXS peaks, increased from 63.1 Å (q = 0.0995 $Å^{-1}$) in the gel phase to 64.5 Å (q = 0.0974 $Å^{-1}$) in the fluid phase. In the Lβ′ phase, WAXS patterns displayed a narrow peak at q = 1.48 $Å^{-1}$ (d = 4.3 Å) with a shoulder at about q = 1.5 $Å^{-1}$ (d = 4.2 Å), characteristic of the quasi-hexagonal packing of the hydrocarbon chains tilted with respect to the bilayer plane. In the Lα phase, a broad bump centered on 1.4 $Å^{-1}$, characteristic of chains in the fluid state, was observed.

Taken together, DSC and WAXS measurements demonstrated that SQ was not inserted between the DPPC acyl chains, perpendicular to the plane of the membrane, since neither the distance between chains, nor their conformation, nor the cooperativity of the transition was modified in its presence. The constant lamellar repeat distance of the SQ-containing samples, even at high molar ratios, also indicated that no significant amount of SQ laid between the two leaflets of the bilayers. In our experimental system, DPPC and SQ therefore coexisted in water as separate phases, with SQ droplets potentially stabilized by a minor DPPC fraction, which would be supported by the observed slight decrease in the DPPC melting enthalpy.

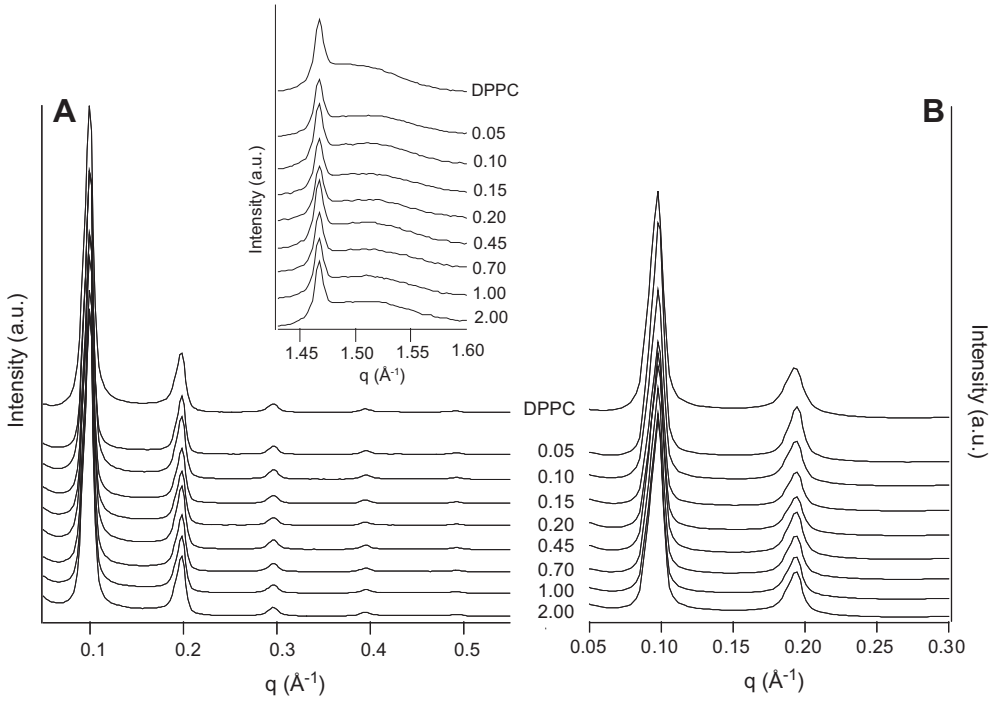

Fig. 6. SAXS patterns of DPPC and SQ/DPPC mixtures at (A) 20 °C, below the transition, and at (B) 50 °C, above the transition. In the insert, the WAXS patterns of DPPC and SQ/DPPC mixtures recorded at 20 °C are shown. The corresponding molar ratio r is indicated on each curve.

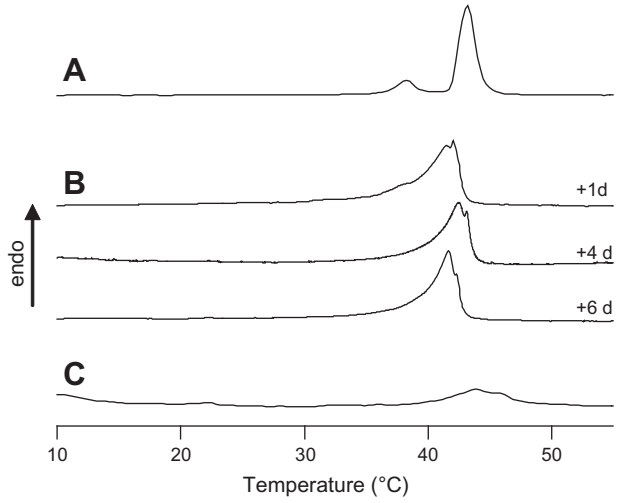

Fig. 7. DSC scans of fully hydrated DPPC (A); SQdFdC NPs/DPPC mixtures recorded after 1, 4, and 6 days of incubation (B); SQdFdC NPs (C), recorded at 2 °C min^{-1}.

Table 2
Thermodynamic data determined by DSC of fully hydrated multilamellar vesicles (MLV) of pure DPPC and of DPPC incubated with SQdFdC NPs.

	T_p onset (°C)	ΔH_p (kJ mol^{-1})	T_m onset (°C)	ΔH_m (kJ mol^{-1})
DPPC	36.9	5.4	42.1	36.7
		Days of incubation	T_m onset (°C)	ΔH_m (kJ mol^{-1})
SQdFdC NPs/DPPC		1	38.3	38.3
		4	40.0	30.2
		6	39.3	34.5

3.5. Interaction of SQdFdC NPs and DPPC liposomes

In a previous study, homogeneous SQdFdC/DPPC mixtures, prepared with a wide range of molar ratios r = [SQdFdC]/[DPPC], had been studied by means of structural (SAXS-WAXS) and calorimetric measurements. With the aim to better mimic *in vitro* experiments, we investigated in the present study whether SQdFdC nanoparticles were able to deliver the prodrug to lipid bilayers across an aqueous medium. Noteworthy, SQdFdC NPs are nanoassemblies inside which SQdFdC molecules are organized in an inverse hexagonal structure [29]. As a consequence, the NPs can take the shape of elongated aggregates, possibly with a diameter of the same order of magnitude than their length, or toroids, formed by closely packed cylinders [30].

Fully hydrated multilamellar vesicles (MLV) of DPPC were incubated in the presence of SQdFdC NPs during 6 days. The molar ratio was 0.09. The evolution of the system was monitored by DSC, SAXS, and WAXS. For this purpose, aliquots of the sample were analyzed after 1, 4, and 6 days. In the absence of molecular exchanges between NPs and bilayers, one would expect to obtain DSC and X-ray curves corresponding to the superimposing of the respective curves of DPPC and NPs. On the contrary, as shown below, the DSC curves and X-ray patterns exhibited features distinct from those of the individual components, indicating that DPPC and SQdFdC formed mixed structures. Fig. 7 shows the DSC curves of SQdFdC NPs/DPPC MLV mixtures recorded after 1, 4, and 6 days of incubation at 37 °C. The thermograms of DPPC and SQdFdC NPs are also displayed for comparison. After exposure to the NPs, the thermodynamic parameters of the DPPC transitions were modified, as summarized in Table 2. The pretransition disappeared, and a broad and asymmetric transition was observed. Interestingly, these curves resemble those of the previously characterized homogeneous SQdFdC/DPPC mixtures in the range $r \sim 0.04$–0.08 [16]. The scatter in T_{onset} and ΔH values of the transition may be

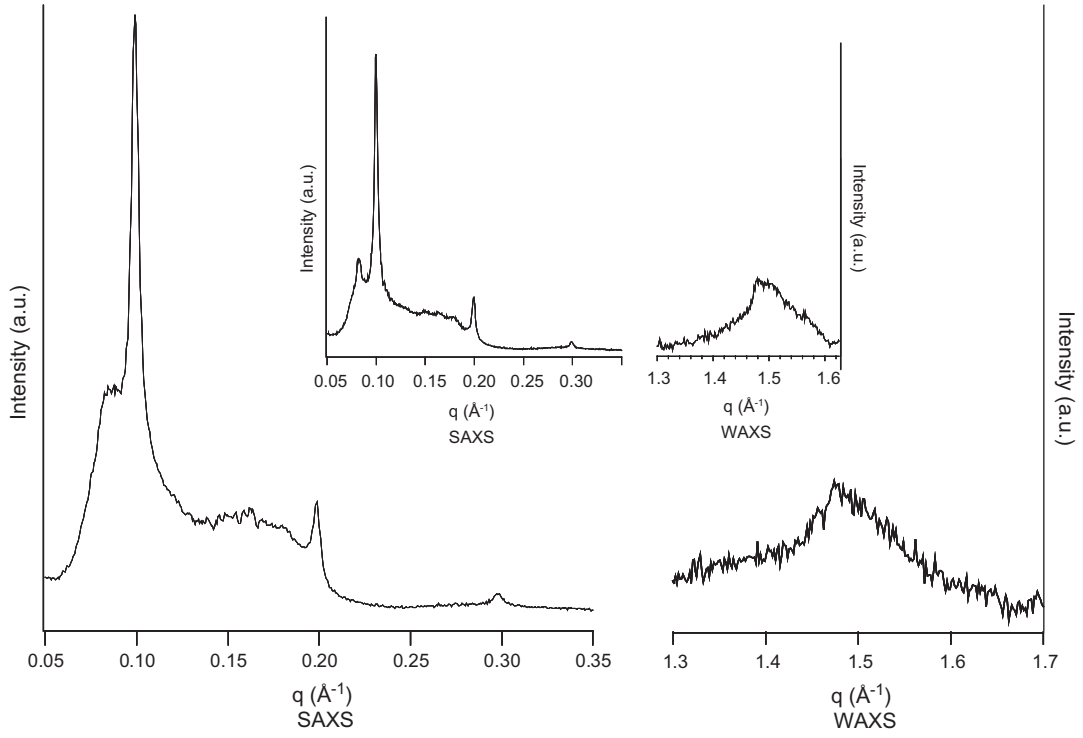

Fig. 8. X-ray diffraction patterns (SAXS and WAXS) of DPPC MLVs incubated with SQdFdC NPs (molar ratio [SQdFdC]/[DPPC] = 0.09), compared to a homogenous SQdFdC/DPPC mixture (molar ratio r = 0.045) after hydration (inset). Data recorded in the gel phase of DPPC, at 20 °C.

attributed to an inhomogeneous diffusion of SQdFdC molecules into DPPC bilayers.

Fig. 8 presents the SAXS and WAXS patterns of a SQdFdC NP/DPPC MLV mixture at a 0.09 molar ratio, recorded at 20 °C (below the transition temperature of DPPC), after 4 days of incubation. They differed from the X-ray patterns of the NPs [29], characteristic of their inverse hexagonal structure, and of pure DPPC (Fig. 6), typical of the Lβ′ lamellar gel phase. Noteworthy, the SAXS and WAXS patterns of the SQdFdC NP/DPPC MLV mixture resembled those of a homogenous SQdFdC/DPPC mixture at molar ratio $r \sim 0.04$ [16], which is displayed in the inset of Fig. 8. Therefore, similar structures were obtained following either hydration of a homogeneous mixture of SQdFdC and DPPC or incubation of DPPC bilayers in the presence of SQdFdC NPs. This suggested the progressive insertion of SQdFdC into DPPC bilayers when SQdFdC NPs were incubated with MLV for several days. The SAXS profile showed a strongly perturbed lamellar phase, as indicated by the presence of a shoulder at $q \sim 0.09$ Å^{-1} ($d \sim 69.7$ Å) and by a diffuse scattering between the two first orders of the lamellar phase at $q = 0.099$ Å^{-1} and 0.198 Å^{-1} ($d = 63.4$ Å). The WAXS profile displayed a broad peak at $q \sim 1.5$ Å^{-1} ($d \sim 4.2$ Å), indicating the loss of extended two-dimensional order of the DPPC chains within monolayers. These patterns were intermediate between those of the lamellar phase and of the inverse bicontinuous cubic phase previously obtained after hydration of a homogeneous mixture of DPPC and SQdFdC for molar ratios $\geqslant 0.08$ [16]. The system could be thought as the coexistence of a lamellar phase and a sponge-like phase, consisting of lamellar sheets randomly joined by water-filled channels [31,32]. The formation of a sponge-like structure with nonuniform negative interfacial curvature could be favored by the inhomogeneous insertion of SQdFdC molecules into DPPC bilayers.

Upon heating at 50 °C, above the main transition temperature of DPPC, a transition to a lamellar phase occurred, consistent with previous experiments on SQdFdC/DPPC mixtures [16]. A peak at $q = 0.095$ Å^{-1} and its second order at $q = 0.19$ Å^{-1}, corresponding to an interlamellar distance of 66.1 Å, were observed (data not shown). In the fluid phase, SQdFdC induced a small increase in the spacing of DPPC.

4. Discussion

Gemcitabine exerts its anticancer activity primarily by impairing DNA synthesis, which results in cytostasis due to a G1- or S-phase block of the cell cycle [33–35]. Cells may then undergo apoptosis or experience mitotic catastrophe upon escaping the cell cycle blockage [36]. The schedule of dFdC's cytotoxic effects has been reported to differ considerably from one cell line to another, depending on their apoptotic machinery and the balance of internal and external pro- or anti-apoptotic factors [37,38]. In the present study, MCF-7, MDA-MB-231, HT-29, and KB-3-1 cell lines strongly responded to dFdC in the 10-nM range. The viability plateau observed above ca. 100 nmol L^{-1} of dFdC indicated that any further drug addition did not decrease the cell viability. On these cell lines, a 48-h incubation with dFdC was, therefore, insufficient for significant cytotoxic effects to occur. On the contrary, the human leukemia cell line CCRF CEM displayed a fully cytotoxic response upon a 48-h exposure to dFdC. The dose–response curve of all cell lines to SQdFdC at concentrations below 10 μmol L^{-1} was qualitatively similar to that of dFdC but occurred at concentrations ca. five times higher. The need for an additional intracellular cleavage step in the case of the squalenoyl prodrug [17] most likely explains this observation. Above 10 μmol L^{-1}, however, on the four cytostatic-responding cell lines that were studied, SQdFdC NPs caused a dramatic cytotoxicity. dFdC supplemented with one equivalent of a SQ dispersion failed to induce the same cytotoxic effect, which indicated that this additional cytotoxicity was caused by SQdFdC rather than by the combination of its hydrolysis by-products.

LDH release assays indicated that high SQdFdC concentrations induced membrane permeation of MCF-7 and CCRF CEM cell lines in a few hours. On the contrary, dFdC did not induce such an effect, even on the CCRF CEM cell line, which displayed a fully cytotoxic response upon a more prolonged exposure to dFdC. Noteworthy, the antimetabolic activity of dFdC is exerted by its triphosphate metabolite [39], which is generated by a time-consuming and self-potentiated phosphorylation process that requires several hours to result in apoptosis [40]. It was, therefore, unlikely that the rapid cell permeation induced by SQdFdC could be attributed to an apoptosis triggered by dFdC intracellularly cleaved from the prodrug. This strongly suggested that the short-term lytic activity of SQdFdC did not come from the antimetabolic activity of dFdC.

As enucleated cells, mammalian erythrocytes are insensitive to the cell cycle effects of dFdC and constituted a valid model to confirm that the cytotoxicity of SQdFdC observed at elevated concentrations came from its amphiphilic properties. As expected, dFdC failed to induce dose-dependent hemolysis, consistently with previous reports indicating that this molecule did not interact with biological membranes under physiological conditions [28]. Squalene alone displayed no hemolytic activity either, which suggested that this compound did not interfere with biological membranes. DSC and SWAXS measurements clearly confirmed this hypothesis. Indeed, they demonstrated that SQ was neither inserted between the DPPC acyl chains, perpendicular to the plane of the membrane, nor between monolayers. This conclusion was consistent with already reported results supporting the absence of effect of SQ on the chain packing of DPPC bilayers [41].

Unlike its hydrolysis by-products, SQdFdC induced a considerable hemolysis, in a time- and dose- dependent fashion. This observation clearly proved that SQdFdC was able to destabilize biological membranes by a mechanism unrelated to the cellular action of dFdC. Taken together, the above-mentioned results suggested that (i) elevated concentrations of SQdFdC permeabilized cellular membranes in a time- and dose-dependent manner, a few hours after administration, (ii) this effect was specifically caused by SQdFdC rather than by the combination of its hydrolysis by-products, and (iii) the lytic activity of SQdFdC was a consequence of the physicochemical properties of the prodrug rather than of the antimetabolic activity of dFdC.

In order to clarify the mechanism of SQdFdC-induced lysis, we investigated whether SQdFdC nanoparticles were able to deliver the prodrug to lipid bilayers in an aqueous medium, by a combination of structural (SAXS-WAXS) and calorimetric measurements. When fully hydrated DPPC bilayers were incubated in the presence of SQdFdC NPs, an exchange was evidenced between NPs and DPPC bilayers over a few days. This confirmed the ability of SQdFdC monomers to be progressively released from NPs and taken up by biomembranes, inducing the perturbation of their supramolecular organization.

Any comparison between *in vitro* assays on cellular models and experiments involving simple lipid bilayers has its shortcomings since real membranes are heterogeneous mixtures of lipids. They exhibit domains of ordered lipids surrounded by a fluid matrix. Moreover, in some cases, the choice of the buffer can affect the behavior of the lipid bilayers [42]. In any case, our observations suggested that, at physiological temperatures, moderate amounts of SQdFdC could actually interact with some lipids, for instance phosphatidylcholines in the gel state, to promote nonlamellar structures.

In this configuration, the bilayers might be perforated by water-filled defects. More importantly, the localized formation of nonlamellar phases in plasma membranes was previously shown to lead to membrane permeation upon exposure to various surface-active agents [18,43]. In this perspective, our hypothesis was that the

mechanism underlying the lytic activity of SQdFdC relied on the insertion of SQdFdC within the cellular membranes, leading to local and transient nonlamellar membrane structures, which caused cytosol leakage and eventually cell death.

In the hemolysis setup, all the SQdFdC concentrations leading to 50% hemolysis corresponded to similar SQdFdC/total lipid ratios. This suggested that the intensity of the lysis was controlled by the value of this ratio. Noteworthy, the 1.2 ± 0.3 SQdFdC/total lipid ratio leading to 50% hemolysis (mean ± SD over the data presented in Table 1) was much larger than the molar ratio threshold of 0.08 required for the formation of nonlamellar structures within hydrated homogenous SQdFdC/DPPC mixtures [16]. Although a threshold determined for DPPC cannot be directly extrapolated to the more complex membranes of red blood cells, this vast discrepancy, however, suggested that a large excess of SQdFdC was required for cell lysis. It is conceivable that the time dependency of the diffusive SQdFdC transfer between NPs and erythrocyte membranes might be responsible for this observation. Indeed, SQdFdC exerted its hemolytic activity in a time-dependent manner, and hemolysis occurred considerably faster in the case of the highest SQdFdC concentrations (Fig. 4), which would result in a faster bioconjugate transfer. Following this line of thought, the hemolysis kinetics should mirror the kinetics of the diffusive prodrug transfer from NPs to erythrocytes. Consistently with the proposed lysis mechanism and experimental measurements, a significant time lapse would therefore be required for an elevated enough insertion of SQdFdC within the membranes to result in the formation of nonlamellar membrane structures, leading to cytosol leakage.

The present study has proven that excessive concentrations of the surface-active SQdFdC could induce cell lysis, in our *in vitro* experimental setups. This mechanism could be the source of side effects such as hemolysis or damage at the site of injection of concentrated NP suspension, *in vivo*. However, it must be emphasized that SQdFdC induced no such toxicity in mice. Indeed, the *in vivo* evaluation of SQdFdC indicated a toxicological profile similar to dFdC [44]. Above the maximal tolerated dose (MTD), SQdFdC neither induced hemolysis nor notably damaged the injection sites in mice and rats, which meant that the lytic properties of SQdFdC were of little consequence in these species. In the scope of the upcoming preclinical evaluation of SQdFdC nanoassemblies on nonrodent animal models, a search for possible signs of hemolysis will be performed and mitigated by adjusting the speed of injection. Anyway, the current clinical practice of chemotherapy strongly emphasizes the use of central venous catheters and implantable venous port systems that maximize the dilution rate of the drugs injected in the bloodstream [45,46]. Such administration routes would most likely mitigate the potential side effects related to the amphiphilic nature of SQdFdC in a clinical perspective.

Acknowledgements

The research leading to these results has received funding from the European Research Council under the European Community's Seventh Framework Programme FP7/2007-2013 Grant Agreement No. 249835. The financial support of the French "Agence Nationale de la Recherche" (ANR, grant SYLIANU) is acknowledged, as well as the doctoral fellowships of LB from the French "Ministère de la Recherche", and of BP from Regione Autonoma Sardegna (Italy). The authors wish to thank Dr. Heinz Amenitsch for his help during X-ray measurements at the synchrotron ELETTRA (Trieste, Italy).

References

[1] A.B. Sandler, J. Nemunaitis, C. Denham, J. von Pawel, Y. Cormier, U. Gatzemeier, K. Mattson, C. Manegold, M.C. Palmer, A. Gregor, B. Nguyen, C. Niyikiza, L.H. Einhorn, Phase III trial of gemcitabine plus cisplatin versus cisplatin alone in patients with locally advanced or metastatic non-small-cell lung cancer, J. Clin. Oncol. 18 (2000) 122–130.
[2] H.A. Burris 3rd, M.J. Moore, J. Andersen, M.R. Green, M.L. Rothenberg, M.R. Modiano, M.C. Cripps, R.K. Portenoy, A.M. Storniolo, P. Tarassoff, R. Nelson, F.A. Dorr, C.D. Stephens, D.D. Von Hoff, Improvements in survival and clinical benefit with gemcitabine as first-line therapy for patients with advanced pancreas cancer: a randomized trial, J. Clin. Oncol. 15 (1997) 2403–2413.
[3] H. von der Maase, S.W. Hansen, J.T. Roberts, L. Dogliotti, T. Oliver, M.J. Moore, I. Bodrogi, P. Albers, A. Knuth, C.M. Lippert, P. Kerbrat, P. Sanchez Rovira, P. Wersall, S.P. Cleall, D.F. Roychowdhury, I. Tomlin, C.M. Visseren-Grul, P.F. Conte, Gemcitabine and cisplatin versus methotrexate, vinblastine, doxorubicin, and cisplatin in advanced or metastatic bladder cancer: results of a large, randomized, multinational, multicenter, phase III study, J. Clin. Oncol. 18 (2000) 3068–3077.
[4] R. Colomer, Gemcitabine and paclitaxel in metastatic breast cancer: a review, Oncology (Williston Park) 18 (2004) 8–12.
[5] R.J. Schilder, J.A. Blessing, M. Morgan, C.E. Mangan, J.S. Rader, Evaluation of gemcitabine in patients with squamous cell carcinoma of the cervix: a Phase II study of the gynecologic oncology group, Gynecol. Oncol. 76 (2000) 204–207.
[6] A.F. Burnett, L.D. Roman, A.A. Garcia, L.I. Muderspach, K.R. Brader, C.P. Morrow, A phase II study of gemcitabine and cisplatin in patients with advanced, persistent, or recurrent squamous cell carcinoma of the cervix, Gynecol. Oncol. 76 (2000) 63–66.
[7] D.F. Moore Jr., R. Pazdur, K. Daugherty, P. Tarassoff, J.L. Abbruzzese, Phase II study of gemcitabine in advanced colorectal adenocarcinoma, Invest. New Drugs 10 (1992) 323–325.
[8] D. Sampath, V.A. Rao, W. Plunkett, Mechanisms of apoptosis induction by nucleoside analogs, Oncogene 22 (2003) 9063–9074.
[9] J. Zhang, F. Visser, K.M. King, S.A. Baldwin, J.D. Young, C.E. Cass, The role of nucleoside transporters in cancer chemotherapy with nucleoside drugs, Cancer Metastasis Rev. 26 (2007) 85–110.
[10] A.M. Bergman, H.M. Pinedo, G.J. Peters, Determinants of resistance to 2′,2′-difluorodeoxycytidine (gemcitabine), Drug Resist. Updat. 5 (2002) 19–33.
[11] J.L. Abbruzzese, R. Grunewald, E.A. Weeks, D. Gravel, T. Adams, B. Nowak, S. Mineishi, P. Tarassoff, W. Satterlee, M.N. Raber, et al., A phase I clinical, plasma, and cellular pharmacology study of gemcitabine, J. Clin. Oncol. 9 (1991) 491–498.
[12] P. Couvreur, B. Stella, L.H. Reddy, H. Hillaireau, C. Dubernet, D. Desmaele, S. Lepetre-Mouelhi, F. Rocco, N. Dereuddre-Bosquet, P. Clayette, V. Rosilio, V. Marsaud, J.M. Renoir, L. Cattel, Squalenoyl nanomedicines as potential therapeutics, Nano Lett. 6 (2006) 2544–2548.
[13] L.H. Reddy, C. Dubernet, S.L. Mouelhi, P.E. Marque, D. Desmaele, P. Couvreur, A new nanomedicine of gemcitabine displays enhanced anticancer activity in sensitive and resistant leukemia types, J. Control Release 124 (2007) 20–27.
[14] L.H. Reddy, H. Ferreira, C. Dubernet, S.L. Mouelhi, D. Desmaele, B. Rousseau, P. Couvreur, Squalenoyl nanomedicine of gemcitabine is more potent after oral administration in leukemia-bearing rats: study of mechanisms, Anticancer Drugs 19 (2008) 999–1006.
[15] L. Bildstein, V. Marsaud, H. Chacun, S. Lepetre-Mouelhi, D. Desmaele, P. Couvreur, C. Dubernet, Extracellular-protein-enhanced cellular uptake of squalenoyl gemcitabine from nanoassemblies, Soft Matter 6 (2010) 5570–5580.
[16] B. Pili, C. Bourgaux, H. Amenitsch, G. Keller, S. Lepetre-Mouelhi, D. Desmaele, P. Couvreur, M. Ollivon, Interaction of a new anticancer prodrug, gemcitabine-squalene, with a model membrane: coupled DSC and XRD study, Biochim. Biophys. Acta 1798 (2010) 1522–1532.
[17] L. Bildstein, C. Dubernet, V. Marsaud, H. Chacun, V. Nicolas, C. Gueutin, A. Sarasin, H. Benech, S. Lepetre-Mouelhi, D. Desmaele, P. Couvreur, Transmembrane diffusion of gemcitabine by a nanoparticulate squalenoyl prodrug: an original drug delivery pathway, J. Control. Release: Off. J. Control. Release Soc. 147 (2010) 163–170.
[18] S. Schreier, S.V. Malheiros, E. de Paula, Surface active drugs: self-association and interaction with membranes and surfactants. Physicochemical and biological aspects, Biochim. Biophys. Acta 1508 (2000) 210–234.
[19] H. Ahyayaucha, M. Gallego, O. Casis, M. Bennouna, Changes in erythrocyte morphology induced by imipramine and chlorpromazine, J. Physiol. Biochem. 62 (2006) 199–205.
[20] A. Jaromin, R. Zarnowski, A. Kozubek, Emulsions of oil from *Adenanthera pavonina* L. seeds and their protective effect, Cell Mol. Biol. Lett. 11 (2006) 438–448.
[21] M. Stasiuk, A. Kozubek, Membrane perturbing properties of natural phenolic and resorcinolic lipids, FEBS Lett. 582 (2008) 3607–3613.
[22] B.N. Erickson, H.H. Williams, S.S. Bernstein, I. Avrin, R.L. Jones, I.G. Macy, The lipid distribution of posthemolytic residue or stroma of erythrocytes, J. Biol. Chem. 122 (1938) 515–528.
[23] H. Jacob, S. Lowry, Membrane lipid depletion in hyperpermeable red blood cells: its role in the genesis of spherocytes in hereditary spherocytosis, J. Clin. Invest. 46 (1967) 2083–2094.
[24] G. Tishkoff, F. Robscheit-Robbins, G. Whipple, Fractions related to experimental conditions red cell stroma in dogs: variations in the stroma protein and lipid, Blood 8 (1953) 459–468.
[25] J. Seydel, M. Wiese, Drug-Membrane Interactions: Analysis, Drug Distribution, Modeling, Wiley-VCH Verlag GmbH & Co, 2002.
[26] J. Virtanen, K. Cheng, P. Somerharju, Phospholipid composition of the mammalian red cell membrane can be rationalized by a superlattice model, Proc. Natl. Acad. Sci. 95 (1998) 4964–4969.

[27] C. Grabielle-Madelmont, R. Perron, Calorimetric studies on phospholipid–water systems: I. – Dipalmitoylphosphatidylcholine (DPPC)–water system, J. Colloid Interface Sci. 95 (1983) 471–482.
[28] B. Pili, C. Bourgaux, F. Meneau, P. Couvreur, M. Ollivon, Interaction of an anticancer drug, gemcitabine, with phospholipid bilayers, J. Therm. Anal. Calorim. 98 (2009) 19–28.
[29] P. Couvreur, L.H. Reddy, S. Mangenot, J.H. Poupaert, D. Desmaele, S. Lepetre-Mouelhi, B. Pili, C. Bourgaux, H. Amenitsch, M. Ollivon, Discovery of new hexagonal supramolecular nanostructures formed by squalenoylation of an anticancer nucleoside analogue, Small 4 (2008) 247–253.
[30] F. Bekkara Aounallah, R. Gref, M. Othman, L.H. Reddy, B. Pili, V. Allain, C. Bourgaux, H. Hillaireau, S. Lepêtre Mouelhi, D. Desmaële, Novel PEGylated nanoassemblies made of self assembled squalenoyl nucleoside analogues, Adv. Funct. Mater. 18 (2008) 3715–3725.
[31] D. Roux, C. Coulon, M. Cates, Sponge phases in surfactant solutions, J. Phys. Chem. 96 (1992) 4174–4187.
[32] M. Baciu, M.C. Holmes, M.S. Leaver, Morphological transitions in model membrane systems by the addition of anesthetics, J. Phys. Chem. B 111 (2007) 909–917.
[33] D. Lorusso, A. Di Stefano, F. Fanfani, G. Scambia, Role of gemcitabine in ovarian cancer treatment, Ann. Oncol. 17 (Suppl. 5) (2006) v188–v194.
[34] P. Cappella, D. Tomasoni, M. Faretta, M. Lupi, F. Montalenti, F. Viale, F. Banzato, M. D'Incalci, P. Ubezio, Cell cycle effects of gemcitabine, Int. J. Cancer 93 (2001) 401–408.
[35] C. Tolis, G.J. Peters, C.G. Ferreira, H.M. Pinedo, G. Giaccone, Cell cycle disturbances and apoptosis induced by topotecan and gemcitabine on human lung cancer cell lines, Eur. J. Cancer 35 (1999) 796–807.
[36] S. Mose, R. Class, H.W. Weber, A. Rahn, L.W. Brady, H.D. Bottcher, Radiation enhancement by gemcitabine-mediated cell cycle modulations, Am. J. Clin. Oncol. 26 (2003) 60–69.
[37] L.J. Ostruszka, D.S. Shewach, The role of cell cycle progression in radiosensitization by 2′,2′-difluoro-2′-deoxycytidine, Cancer Res. 60 (2000) 6080–6088.
[38] P. Hernandez, P. Olivera, A. Duenas-Gonzalez, M.A. Perez-Pastenes, A. Zarate, V. Maldonado, J. Melendez-Zajgla, Gemcitabine activity in cervical cancer cell lines, Cancer Chemother. Pharmacol. 48 (2001) 488–492.
[39] P. Huang, S. Chubb, L.W. Hertel, G.B. Grindey, W. Plunkett, Action of 2′,2′-difluorodeoxycytidine on DNA synthesis, Cancer Res. 51 (1991) 6110–6117.
[40] V. Heinemann, Y.Z. Xu, S. Chubb, A. Sen, L.W. Hertel, G.B. Grindey, W. Plunkett, Cellular elimination of 2′,2′-difluorodeoxycytidine 5′-triphosphate: a mechanism of self-potentiation, Cancer Res. 52 (1992) 533–539.
[41] S.A. Simon, L.J. Lis, R.C. MacDonald, J.W. Kauffman, The noneffect of a large linear hydrocarbon, squalene, on the phosphatidylcholine packing structure, Biophys. J. 19 (1977) 83–90.
[42] T. Peiro -Salvador, O. Ces, R.H. Templer, A.M. Seddon, Buffers may adversely affect model lipid membranes: a cautionary tale, Biochemistry 48 (2009) 11149–11151.
[43] E. Prenner, R. Lewis, K. Neuman, S. Gruner, L. Kondejewski, R. Hodges, R. McElhaney, Nonlamellar phases induced by interaction of Gramicidin S with lipid bilayers; a possible relationship to membrane-disrupting activity, Biochemistry 36 (1997) 7906–7916.
[44] L.H. Reddy, P.E. Marque, C. Dubernet, S.L. Mouelhi, D. Desmaele, P. Couvreur, Preclinical toxicology (subacute and acute) and efficacy of a new squalenoyl gemcitabine anticancer nanomedicine, J. Pharmacol. Exp. Ther. 325 (2008) 484–490.
[45] S. Vescia, A.K. Baumgartner, V.R. Jacobs, M. Kiechle-Bahat, A. Rody, S. Loibl, N. Harbeck, Management of venous port systems in oncology: a review of current evidence, Ann. Oncol. 19 (2008) 9–15.
[46] M. Gallieni, M. Pittiruti, R. Biffi, Vascular access in oncology patients, ACS Online CE 58 (2008) 323–346.